J. Fluid Mech. (1983), *vol.* 135, *pp.* 355–371
Printed in Great Britain

An evaluation of some collision models used for Monte Carlo calculations of diatomic rarefied hypersonic flows

By J. DAVIS†, R. G. DOMINY‡, J. K. HARVEY AND M. N. MACROSSAN
Department of Aeronautics, Imperial College, London

(Received 8 February 1983)

Three intermolecular collision models have been used in Monte Carlo direct-simulation computations. Their merits have been assessed by comparing the predictions given for two contrasting flows with experimental results. In one flow viscous effects were predominant; in the other the rapid compression ahead of a blunt body was the feature concentrated upon. In both examples the flows were rarefied and hypersonic and the gas was diatomic and rotationally excited.

1. Introduction

The Monte Carlo direct simulation method (Bird 1976) is an established technique for computing viscous flow fields where non-equilibrium effects due to rarefaction make the Navier–Stokes equations inappropriate. The method assumes that the motion of several thousand particles can adequately 'simulate' that of a far larger number of real molecules. These simulation particles exist within a framework of cells and carry with them phase space information of position, velocity and internal energy. The full Boltzmann equation is applied directly to the particles by decoupling the convection and collision terms by a suitable time discretization and each is calculated alternately in the time interval independently of the other.

Using the technique various solutions have been obtained for rarefied flows (Knudsen number > 0.01) usually for high incident Mach numbers. Because of the complications introduced by internal energy exchange, the earlier investigations were restricted to monatomic gases, and, although now many possible collision kernels have been developed to deal with polyatomic encounters ranging from empirical to fully quantum-mechanical treatments, the problem remains of selecting ones suitable for inclusion in the Monte Carlo simulation. A careful balance between precision and efficiency is crucial since the algorithm may be used millions of times in a typical computation. In this paper practical examples for diatomic gases are assessed by comparing the results from computed flow fields with data obtained experimentally.

The collision calculations can be separated into two parts by treating the molecular inelasticity as an energy transfer superimposed upon the spherical scattering process. This has been justified in a perturbation analysis by Pullin (1974), who showed that the inelastic corrections to the elastic deflection angles appear as second-order quantities. The pair collision probability and deflection angles can thus be computed from monatomic collision dynamics independently of the internal energy.

† Present address: HMS 'Daedalus', Lee-on-Solent, Hampshire, UK.
‡ Present address: Whittle Laboratory, Cambridge.

2. The collision modelling

The collision formalisms now available for diatomic molecules are of two types: *impulsive models*, employing approximations to classical or quantum-mechanical representations of the collision, and *phenomenological models*, in which local relaxation concepts are used to calculate the energy exchange processes for individual encounters. A variety of intermolecular potentials has been used with these models to calculate the trajectories.

Early impulsive formulations include the 'rough-sphere' model (Bird 1970*a*), which inadequately represents diatomic effects, Jean's 'loaded-sphere' model further developed by Melville (1972), and Parker's (1959) 'non-spherical soft-molecule' model used by Macpherson (1971), which gives a more realistic representation of the energy exchange but incurs computing time prohibitive for it to be used for anything but the simplest flows. The approximation to this model used by Pullin (1974), which he hoped retained the physical characteristics of the full model, did not satisfy detailed balancing sufficiently well to produce acceptably near equipartition at equilibrium. He had to introduce *ad hoc* corrections to force equipartition.

More recently quantum-mechanical formalisms have appeared, but these invoke similar criticisms to the classical procedures. Deiwert & Yoshikawa (1975), who were concerned with low temperature ($\sim$ 10 K), were able to use a semiclassical method based on the Pearson–Hansen (1972) model. This employs point centres of repulsion for the collision dynamics and the Schrödinger equation for a rigid-rotator harmonic oscillator to compute the rotational energy transition probabilities. However, as with Pullin, simplifying semiempirical modifications had to be incorporated to make the model tractable for Monte Carlo calculations. Reasonable equipartition is achieved up to a temperature of 320 K, but thereafter it breaks down.

Itikawa & Yoshikawa (1975) have developed a more realistic quantum-mechanical model based on the inverse-power potential. Well-behaved relaxation tests are obtained by optimizing against the exponent α of the intermolecular potential. Although an advance on Deiwert's model, it is extremely time-consuming and it is unlikely that the bulk properties, such as viscosity, will be adequately predicted by this method of choosing α. Neither paper makes reference to the variation of molecular elasticity with temperature.

The principal disadvantage of the classical and quantum-mechanical models is that they are either unacceptably artificial or excessively demanding of computing time. Alternative methods using phenomenological modelling of the internal energy transfer to avoid the complex inelastic collision dynamics have been proposed by Bird (1970*b*) and Borgnakke and Larsen (Borgnakke & Larsen 1973; Larsen & Borgnakke 1974). In Bird's *energy-sink* method, the exchange operates so as always to drive the pair internal and translational energies towards local equilibrium. Although guaranteeing macroscopic equilibrium the model is unrealistic, not satisfying detailed balancing, since all collisions are forced in the direction of equilibrium.

In their two papers, Borgnakke & Larsen proposed statistical extensions to Bird's idea. In the first, individual collisions were treated as fully inelastic with probability ϕ, or completely elastic with probability $1-\phi$. The constant ϕ is called the *exchange restriction factor*. During the inelastic collisions, the total energy is redistributed between the translational and rotational modes according to probabilities derived from the equilibrium distribution. This model was used by Pullin to replace the original *ad hoc* corrections to his approximate classical model. For high-energy collisions the impulsive calculation is retained, while low-energy collisions are treated

statistically (Pullin & Harvey 1976). Some results using this *hybrid model* are presented in this paper. In their second paper, Borgnakke & Larsen (1974) extended the statistical exchange model by dividing the total centre of mass energy e_{cm} into two fractions for every collision. A fraction $(1-\phi)\,e_{cm}$ is treated elastically, while the remainder undergoes an inelastic exchange where the energy is reapportioned in a similar statistical manner to that of the first model. The components are then combined to give the post-collision velocity and internal energy. This *restricted exchange scheme* is an improvement on the first since a more realistic collision is calculated each time instead of one of two notional extremes.

Simulated relaxation calculations have been made using the restricted exchange scheme combined with deflections calculated using the inverse-power potential

$$U(r) = \beta/r^{\alpha}, \tag{1}$$

where r is the distance from the molecule centre and α was selected as 13.5 to give the best fit for the viscosity data for nitrogen (Wooley 1956) at temperatures above 250 K.

Detailed classical calculations with Parker's diatomic molecule indicate that an appreciable amount of rotational energy is exchanged only in close encounters (Lordi & Mates 1970). To simulate this no exchange of internal energy is allowed for those collisions where the dimensionless impact parameter $\Delta(= b(mg^2/2\alpha\beta)^{1/\alpha}) > 1$, which corresponds to deflections of less than 0.31 rad. The 'inelastic cross-section' is thus smaller than the total collision cross-section which was chosen to include deflections greater than 0.05 rad. The interdependence of ϕ and the rotational collision number Z_R is found to be well approximated by the simple expression

$$Z_R = 1.624/\phi^{0.978} \quad (0.1 < \phi < 1.0). \tag{2}$$

The relaxation simulations were performed on an ensemble of particles which had initially a Maxwellian distribution of translational energy and zero rotational energy. Z_R was obtained from a best fit to an exponential decay of the form

$$\frac{T_t - T_R}{(T_t - T_R)_{\text{initial}}} = exp\left(-\frac{5\hat{t}}{3Z_R}\right), \tag{3}$$

where subscripts t and R refer to translational and rotational quantities respectively and $\hat{t}$ is the time normalized with respect to the nominal mean collision interval. Equipartition was not accurately achieved even after a long time, the rotational temperature being consistently about 3 % below the translational.

Pullin (1975) has analysed in detail the construction of statistical collision kernels with a specific regard to the Boltzmann equation and the ability to construct H-theorems from the kernels. He showed that this model does not satisfy the principle of detailed balance. However, the model offers practical advantages in being simple to use, simulating the correct number of degrees of freedom and producing an acceptable approximation to equipartition at large time. Against this, the pre- and post-collision properties are uncorrelated for each encounter. More seriously, since ϕ is set constant, no account is taken for variation of rotational relaxational rate from encounter to encounter or from point to point within the flow field. Figure 1 shows some theoretical predictions for $Z_R(T)$ for nitrogen and the measured values of Carnevale, Cary & Larsen (1967). It can be seen from these that ϕ should vary considerably if the simulation is to reproduce this behaviour. Pullin (1975) showed, for a restricted exchange scheme similar to Borgnakke and Larsen's, that the model would satisfy detailed balance if ϕ varied for each collision as a function of any

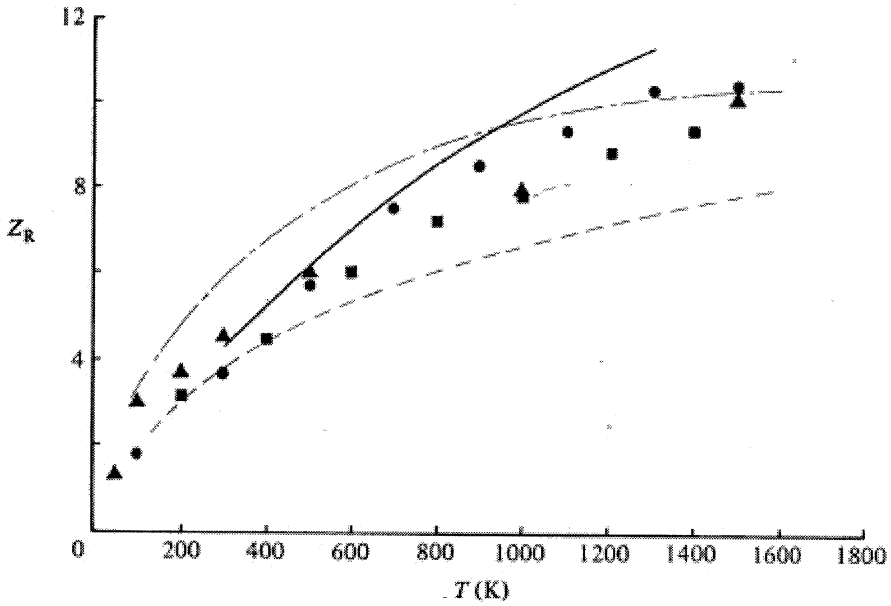

FIGURE 1. Rotational collision number for nitrogen. Experiment: ——, Carnevale *et al.* (1967). Theoretical predictions: – – –, Parker (1959); – · – · –, Lordi & Mates (1970). Monte Carlo: ●, variable-ϕ inverse-power; ▲, hybrid Morse potential; ■, variable-ϕ Morse potential.

property which was the same for the inverse as for the forward collision. As a first step then, a kernel was proposed by Davis and Pullin (Davis 1978) in which ϕ is a function of $e_{\rm cm}$. Using his corrected version of the restricted exchange scheme, Pullin (1978) related ϕ to $Z_{\rm R}$ using the Wang–Chang and Uhlenbeck extension of the Chapman–Enskog method (Hirschfelder, Curtis & Bird 1965, p. 501). For the inelastic cross-section described above and constant ϕ these results predict $Z_{\rm R} = 1.736/\phi$, which is close to our equation (2). Using the Carnevale data and the theoretical results, Pullin proposed that for nitrogen ϕ for each collision should be

$$\phi(\hat{e}) = 0.148 + \exp\left[-1.722 \times 10^{-3}\hat{e}\right] \tag{4}$$

where $\hat{e} = e_{\rm cm}/2k$ and k is Boltzmann's constant. We refer to this as Pullin's *variable-ϕ model*. From relaxation calculations using (4), the rotational collision number was determined for different temperatures. The results shown in figure 1 are in reasonable agreement with the measured data despite the departure from equilibrium being greater than that for which the Chapman–Enskog theory could resonably be expected to succeed. The values of $Z_{\rm R}$ calculated using Pullin's hybrid model are also shown in the figure.

Two further types of relaxation simulation have been examined. In type A the temperature history is followed for a molecule ensemble which starts with equilibrium distributions of both translational and rotational energies. In type B the molecules start with equal temperature components but different distributions. The initial velocity distribution is Maxwellian, but the rotational energy is distributed as a delta function. Figure 2 shows a typical type-A result for the variable-ϕ model. Equipartition at equilibrium is not exact, the energy transfer from rotation to translation being preferred. Similar results were observed for the constant-ϕ model; however, a closer agreement with the Maxwellian distribution is achieved with the variable-ϕ model.

The redistribution of the rotational energy in the type-B relaxation is shown in figure 3. The energy is divided into six bands in the range 0 to $1.475kT$. A very rapid decay towards an equilibrium distribution is seen. This is because, in the

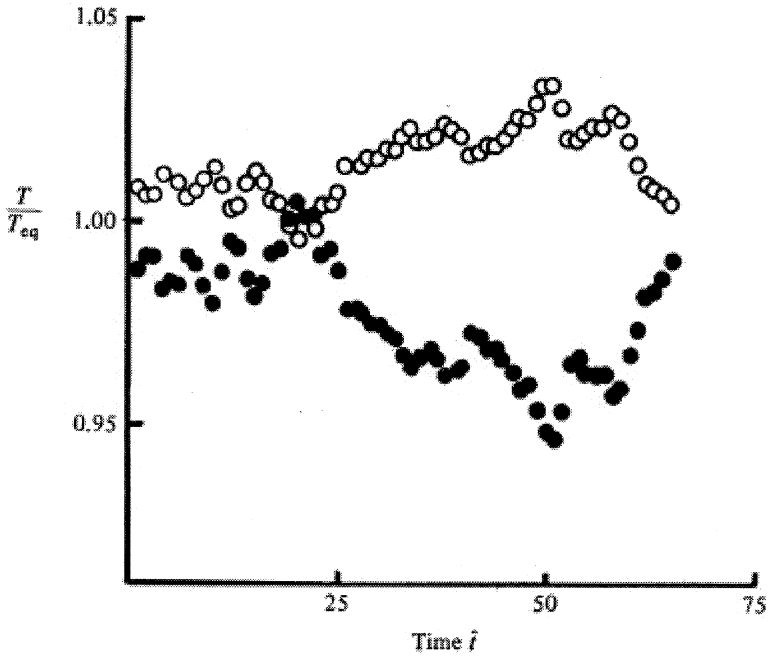

FIGURE 2. Temperature history for a type-A stability test using variable-ϕ inverse-power model. Equilibrium temperature $T_{eq} = 1000$ K. ○, Translational temperature; ●, rotational temperature.

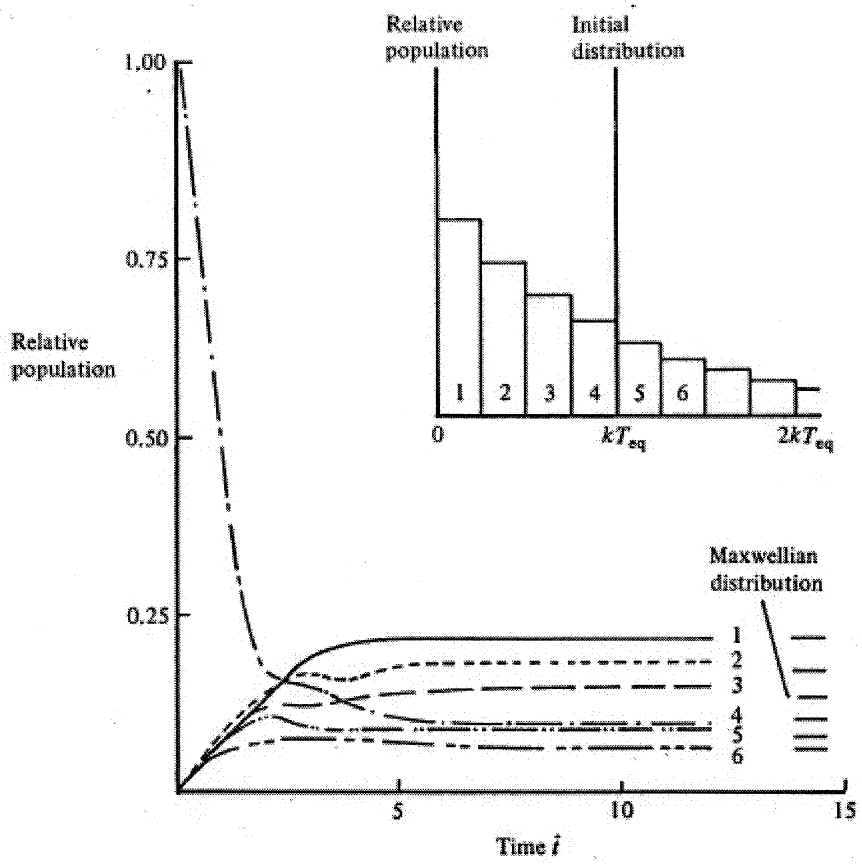

FIGURE 3. Relaxation of rotational energy distribution. Variable-ϕ inverse-power model. Type-B test.

phenomenological models so far considered, the post-collision rotational energy is randomly redistributed between the two molecules according to the equilibrium distribution $\exp(-e_R/kT)$. Pullin (1975) proposed including into a model a second parameter like ϕ to characterize this internal energy relaxation. By ignoring this, the postcollision rotational energy is forced towards equilibrium with a collision number of about 1. The authors are unaware of experimental work which could lead to a determination of this new parameter, but estimates could be made using results from accurate classical modelling. Similar difference in the temperature components after a long time were noted in both type-A and type-B tests.

In addition to the inverse 13.5 potential, the Morse potential was used to determine the scattering. Originally proposed by Morse (1929) as a realistic representation of the binding energy for simple atoms, it also appears in the first-order perturbation solution for Parker's diatomic molecule. It includes a long-range molecular attraction and in a form corresponding to the more well-known Lennard–Jones potential is

$$U(r) = 4kT'\left[\exp\left\{-a\left(\frac{r}{\sigma}-1\right)\right\}-\exp\left\{-\frac{a}{2}\left(\frac{r}{\sigma}-1\right)\right\}\right]. \tag{5}$$

The first approximation to the viscosity in the Chapman–Enskog transport theory is

$$\mu(T) = \frac{5(mkT/\pi)^{\frac{1}{2}}}{16\sigma^2\Omega^{(2,2)*}}, \tag{6}$$

where $\Omega^{(2,2)*}(T/T')$ is a collision integral (Hirschfelder *et al.* 1965). Pullin (1974) has calculated this integral for the Morse potential with $a = 14.798$. With $\sigma = 3.681$ Å and $T' = 91.5$ K, the viscosity from (6) is in good agreement with the nitrogen data in the range $150\text{ K} < T < 1500\text{ K}$.

For low collision energies, the molecules can orbit each other. This leads to a singularity in the calculated deflection angle which was avoided by substituting the deflection angle for a collision with initial conditions only slightly different from those which gave the singularity. The collision cross-section was selected to include these collisions which are important in establishing the low-temperature viscosity. When this collision model was combined with the variable-ϕ model, inelastic cutoff was applied when $b > \sigma$, which was the cutoff condition carried over from the hybrid model. This gives an inelastic collision rate different from that for the inverse power potential. Thus the values of Z_R are slightly different at high temperatures (see figure 1). Since the deflection angle within this inelastic cross-section is not a single-valued function of Δ, it follows from Pullin's (1978) analysis that the Morse-potential variable-ϕ combination cannot satisfy the principle of detail balance even when a corrected restricted exchange is used. It appears from experience, however, that the extra error is masked by the small error in the original restricted exchange scheme used here.

3. The experiments

To assess the accuracy of the variable-ϕ and hybrid models in practical situations, comparisons have been made between computations and experimental measurements for two body shapes in rarefied hypersonic nitrogen flow. Surveys of flow-field density and, in some cases, rotational temperatures have been made using the electron-beam fluorescence technique. This is a non-intrusive method that avoids the interference caused by physical probes which, in rarefied flows, can be excessive. Other data, such

as surface pressures, have not been used to evaluate the results of the computations because the necessity of applying large correction factors to these leads to experimental uncertainties that are too large.

The body shapes in these experiments were chosen with regard to minimizing experimental error. The first flow was one in which viscous effects were to dominate. The conventional choice would be a 'two-dimensional' flat plate at zero angle of attack. However, this configuration is dogged by undesirable three-dimensional flow effects which are especially troublesome in the rarefied regime. These unquantifiable errors were avoided by using the axisymmetric equivalent of the flat plate, the outer surface of a sharp hollow cylinder aligned with its axis of symmetry into the flow.

The Monte Carlo method is reputedly suspect where the flow is rapidly decelerated. For this reason, amongst others, the second case was chosen as a flat-ended circular cylinder with its axis aligned with the flow. This provided a simple example of deceleration and is a marked contrast to the first flow. The rapid rise of temperature ahead of the front face should highlight any differences between the variable-ϕ and hybrid collision models.

All the experiments were conducted in the Imperial College Hypersonic Nitrogen Wind Tunnel, which operates in the Mach-number range of 20–24. Free-stream mean free paths λ_∞ of 0.5 mm can be achieved within the test section, which is 200 mm in diameter (Harvey, Jeffery & Uppington 1971). The models were water cooled and made to high standards from a tellurium–copper alloy. The blunt cylinder was 10 mm in diameter. The hollow cylinder was 44 mm in diameter at the leading edge and 150 mm long. The leading edge was sharp and chamfered at 10° at the inner surface and the outer surface was given a slight outward taper of 1°. This compensated, in some measure, for the conicity of the undisturbed tunnel flow which had a 1° outflow at the model's leading edge. Both models were supported at the rear, and an unchoked supersonic flow was established through the centre of the hollow cylinder. The hollow cylinder was constructed with sharp-lipped pressure tappings, 0.4 mm in diameter, along its length but, for the reasons already stated, results from these are not used here. However, four tappings equally spaced around the model at one axial station were used to verify that it was accurately aligned with the flow.

The electron-beam fluorescence technique used for the flow surveys has been fully described by Muntz (1961). A well-collimated beam of electrons was fired into the gas from a 30 kV source outside the tunnel. This caused a fluorescent glow, the intensity of which at points along the beam gave a measure of the gas density. The rotational temperature was inferred from the detailed vibrational–rotational band structure of the near-ultraviolet spectrum of the emitted light. Because the light levels were low, a digital acquisition and processing technique was used to improve the signal-to-noise ratio and to resolve and correct the spectra. Details of the method are given by Davis & Harvey (1979). It is estimated that the maximum error in measuring the density is $\pm 4\,\%$. There are systematic errors in inferring the rotational temperature from the spectrum which are unquantifiable because, for example, it is not known how far the distribution of rotational energy departs from the Boltzmann distribution which is assumed when reducing the data (Davis 1978). There is a random error of $\pm 5\,\%$. For the blunt cylinder the conventional approach of firing the beam from beneath the surface of the model through a small hole was used. As the region of interest lay ahead of the front face, the beam was deflected magnetically into the flow direction to emerge from the model through a 0.5 mm orifice, the radial position of which could be varied. Just beneath the surface the beam passed through a cavity within which the pressure was controlled to balance the external pressure to minimize

the flow in or out of the orifice. This complicated technique was chosen rather than the simpler arrangement of firing the beam across the front of the model as it was considered that passing a beam parallel and close to a conducting surface significantly distorts the secondary electron cloud which extends some distance from the main light-emitting beam. As the secondary electrons play an important role in the fluorescence, unquantifiable distortion of their distribution may affect the validity of the light intensity–density calibrations.

For the hollow cylinder a different beam arrangement was adopted. A thin (0.15 mm) layer of graphite, which has the property of trapping incident electrons, was embedded in the model surface, making it possible to fire the beam directly at the model without giving rise to an increased glow near the surface from the reflected secondaries. Careful evaluation at constant densities showed that this method gave rise to smaller errors than the conventional arrangement, but the distance from the surface over which a correction had to be made extended further to about $2\lambda_\infty$. A high-thermal-conductivity adhesive was used to hold the graphite, and a surface temperature rise of < 0.3 K was estimated due to aerodynamic heating. A spatial resolution of 0.15 mm in the beam direction was achieved in all experiments. All readings were corrected for variations in beam current.

4. Boundary conditions

With the numerical method being used here it is not necessary to restrict the calculations to a uniform incidence stream. The upstream boundary conditions can be set to match those measured in the appropriate planes in the wind-tunnel flow with their inevitable non-uniformities. This was done using Pitot and yawmeter data, first for the empty test-section flow and then for the hollow-cylinder flow. The former was done to test the realism of the approach and close agreement was obtained between the measured and calculated values of Mach number as the flow progressed along the tunnel.

The nominal mean free paths in the freestream can be calculated from viscosity using the relation

$$\lambda(T) = \frac{32\mu(T)}{5\pi\rho\bar{c}}, \tag{7}$$

where $\bar{c}$ is the mean thermal speed in an equilibrium gas and ρ is the density. In these experiments the freestream temperature was of the order of 10 K and the quoted mean free paths were derived using viscosity calculated with (6), the collision integrals for the Lennard–Jones potential (Hirschfelder *et al.* 1965), and the values of σ and T^* given above.

In all computations, diffuse scattering of particles from the body surfaces, fully accommodated to the surface temperature, has been assumed.

5. Hollow-cylinder results

Representative samples taken from the electron-beam density profiles, measured at different streamwise stations on the hollow cylinder, are compared in figure 4 with the simulation computations using the variable-ϕ model with the inverse-power and Morse potentials, and the hybrid model with the Morse potential. Direct quantitative comparisons cannot be made with the flat-plate data from the literature since in the axisymmetric flow the shock is weaker and nearer the surface. There is, however, a

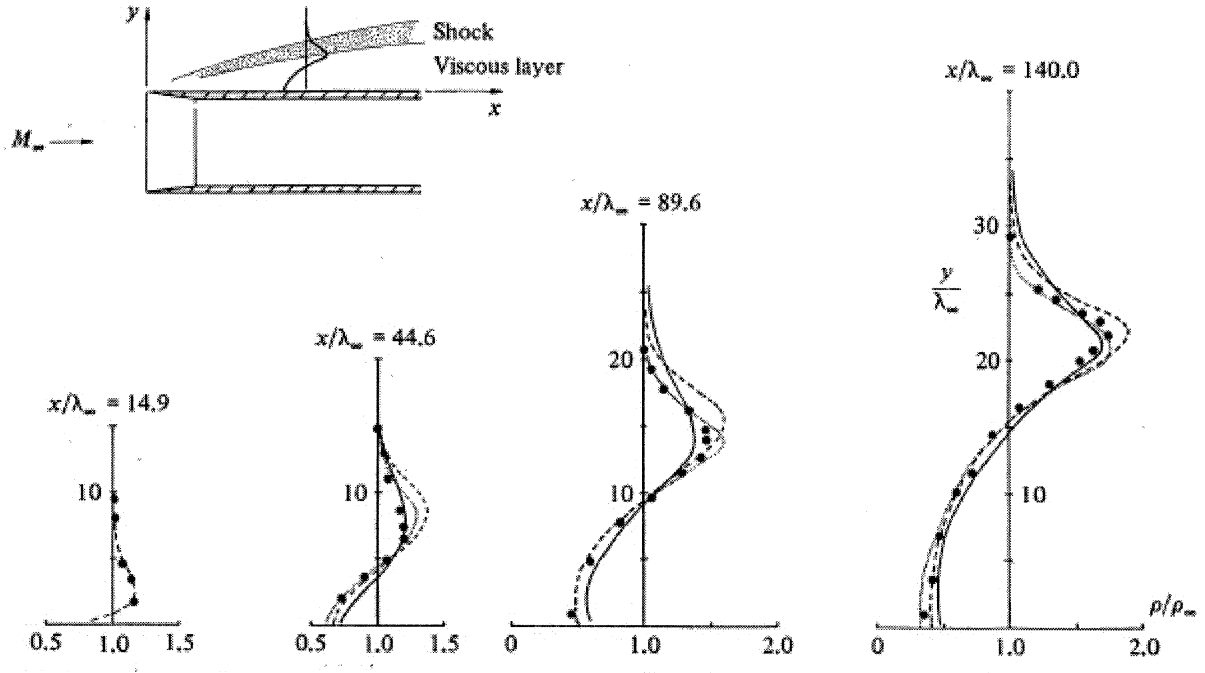

FIGURE 4. Hollow-cylinder density profiles. $M_\infty = 20.7$, $T_w/T_\infty = 13.8$, $\lambda_\infty = 0.33$ mm, $T_0 = 2000$ K. ●, Experimental results. Computed values: - - -, variable-ϕ Morse potential; ..., hybrid Morse potential; ——, inverse-power variable-ϕ.

close qualitative similarity (Davis 1978, figure 56). The flow develops from a 'kinetic region' around the leading edge into a 'fully merged' shock and viscous layer further downstream. The shock, which is produced by the displacement effect of the viscous layer, has a substantial thickness. Within it the density rises steeply to a peak which is less than the equivalent Rankine value for a shock at the same angle. This is because of the interference to its structure by the non-equilibrium viscous layer that fills the space between it and the body surface.

From figure 4 it is evident that the Morse potential gives better overall agreement with the data than the inverse-power potential. The results for the latter show the flow developing more slowly, with smaller gradients and a weaker shock, than was measured. The structure of the shock in particular is poorly represented. In contrast, the development of the viscous sublayer and the structure of the shock are well matched by the Morse potential. This is thought to be because the Morse potential gives a better prediction of viscosity over a wide temperature range than the inverse power potential. The choice of parameters for the latter gives high values of viscosity at temperatures below 250 K. The inverse-power density profiles can be made to match the experimental results more closely in the viscous layer by normalizing against a larger mean free path (in effect by changing the constant β which is a measure of the 'size' of the molecule).

Near the front of the flow within the kinetic region ($x/\lambda_\infty = 14.9$) the experimental results agree closely with all the simulations. Only one curve has been drawn through the data since the profiles coincide within the statistical scatter. The density peak for the hybrid model is perhaps an exception, being slightly higher than the others. Both the variable-ϕ and hybrid models work well, but the impulsive part of the hybrid model, which is expected to be an important feature within this region, may account for this slight departure from the other results.

As the flow develops into the merged region, the differences between the variable-ϕ and the hybrid models, incorporating the Morse potential, become clear from the position and strength of the density peak. Since the merged layer is essentially a matching between the strongly interacting viscous boundary layer generated by the body-reflected particles and the non-Rankine–Hugoniot shock, the conditions just downstream of the shock (as measured by the peak density) are a very sensitive indicator of the method's precision. Both models predict a higher peak than was measured near the front of the flow, but the hybrid value increases slowly and so matches the amplitude of the experimental value by $x/\lambda_\infty = 140$. The variable-ϕ gives a larger peak than the hybrid and the shock is always further from the body than in the measured flow. In the shock the density gradients are well matched by both models. It can be concluded that, with the Morse potential, both variable-ϕ and hybrid models perform well, there being a slight preference towards the classical hybrid model.

Rotational temperature measurements for the body were in broad agreement with the numerical predictions, but because of experimental difficulties the likely errors were too large for any conclusions to be drawn about the merits of the collision models (see Davis 1978).

6. Blunt-cylinder results

The second body shape for which comparative data are presented is the flat-ended circular cylinder. Here the emphasis was on assessing the behaviour of the Monte Carlo scheme where the gas was compressed rapidly.

In supersonic flow at high Reynolds numbers such a body generates a strong near-plane shock wave ahead of its front face. Behind this shock there is a region of subsonic radial outflow which is essentially inviscid and a thin viscous layer adjacent to the surface. A sonic line extends from the corner of the body to the shock, and beyond this line there is a rapid supersonic expansion of the fluid as it flows from the front face down the sides of the cylinder. An overexpansion, due to the formation of a small separation bubble at the sharp corner followed by an embedded shock, has been noted. The effect on the flow of reducing the Reynolds number is to thicken the viscous layer and the shock until eventually the two merge in front of the body, producing a continuous compression up to the front face. All the examples presented in this paper are for situations where this merging has occurred.

Density contours taken from representative examples of the computed fields using the variable-ϕ Morse potential model are shown in figure 5. The steady rise in density as the front face is approached and the expansion around the corner are both evident. Near-axis streamwise density and temperature profiles, calculated for a range of Knudsen numbers Kn_R based on the cylinder radius R, are presented in figures 6 and 7. As the front face of the body is approached, the density rises steadily to a value that is more than twice that for the equivalent continuum inviscid flow. Even for the least-rarefied flow, $Kn_R = 0.0465$, there is no indication from the density profiles of a discrete shock being formed although there is a rapid rise in the translational temperature characteristic of a shock. This occurs further from the body than the shock stand-off distance predicted for an inviscid continuum flow (Vinokur 1959) and before any appreciable rise in density. In each case the rise in rotational temperature lags far behind the translational temperature. Consequently, for the denser flows the translational temperature rises above the continuum value for a diatomic gas before dropping towards the surface temperature near the body. The

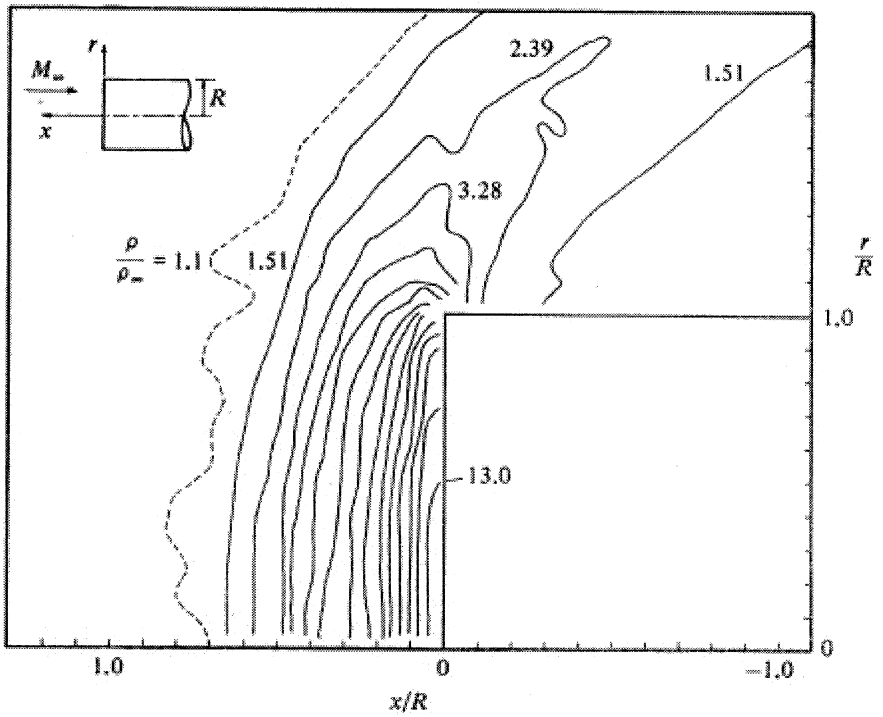

FIGURE 5. Density contours for the blunt-ended circular cylinder using the variable-ϕ Morse potential. Contours equally spaced from $\rho/\rho_\infty = 1.51$–13.0. $M_\infty = 20.6$, $Kn_R = 0.0282$, $T_0 = 1405$ K.

difference between the two temperatures diminishes as the collision rate increases and Kn_R decreases. Estimates of the average number of collisions along streamlines indicate that, for all but a negligible number of particles arriving very close to the stagnation point, vibrational energy exchange cannot play an important role in determining the flow field.

A set of streamwise density profiles for different radial positions is presented in figure 8 for $Kn_R = 0.0648$, which corresponds to the conditions at which the density measurements were obtained. The Mach number was 25.4 and the body- to stagnation-temperature ratio was 0.26. A line has been faired through each set of measured points which show very little scatter. Numerically predicted values of density for each collision model are plotted as points. For much of the flow field there is close agreement between the measured and computed values and the variable-ϕ inverse-power model appears to give the most accurate prediction. This is in contrast to the hollow-cylinder flow, where this model gave the poorest results. In this flow the scattering dynamics of encounters between freestream and body-reflected particles must be important. The scattering for these high-energy collisions will be similar for the inverse-power and Morse potentials, and it is likely that the cutoff procedure applied to the latter is at fault. Since the temperatures within the flow field are high, the region where the inverse power gives poor viscosity predictions will be, for the most part, avoided. Generally the error in predicted density is not large and the high values close to the body surface are well reproduced. The greatest discrepancies are near the axis between the peaks of translational and rotational temperatures ($0.5 > x/R > 0.25$).

The difference in the inelastic cutoff conditions for the energy-exchange models could also be important. For the inverse-power potential the inelastic cutoff is based on the non-dimensional impact parameter Δ. It is natural then to apply the same

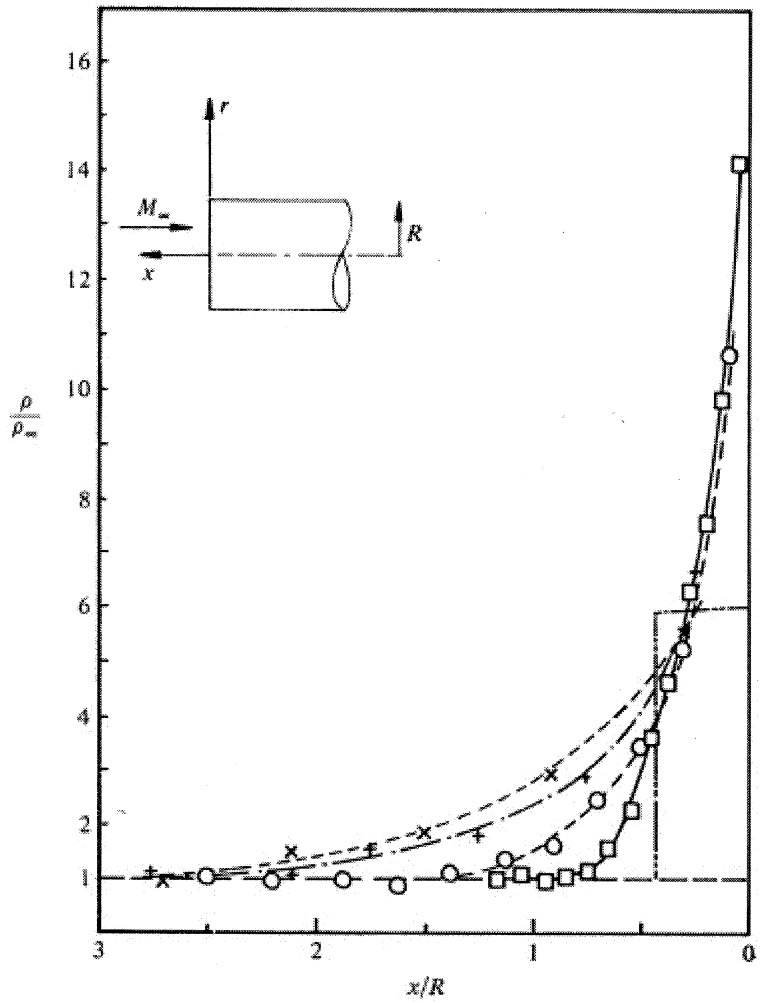

FIGURE 6. Computed near-axis density profiles for blunt-ended cylinder. $M_\infty = 24.77$, $T_w/T_0 = 0.26$, $T_0 = 1446$ K. Variable-ϕ Morse potential. ×, $Kn_R = 1.840$; +, 0.613; ○, 0.306; □, 0.0465; – – –, continuum inviscid result, $\gamma = 1.4$.

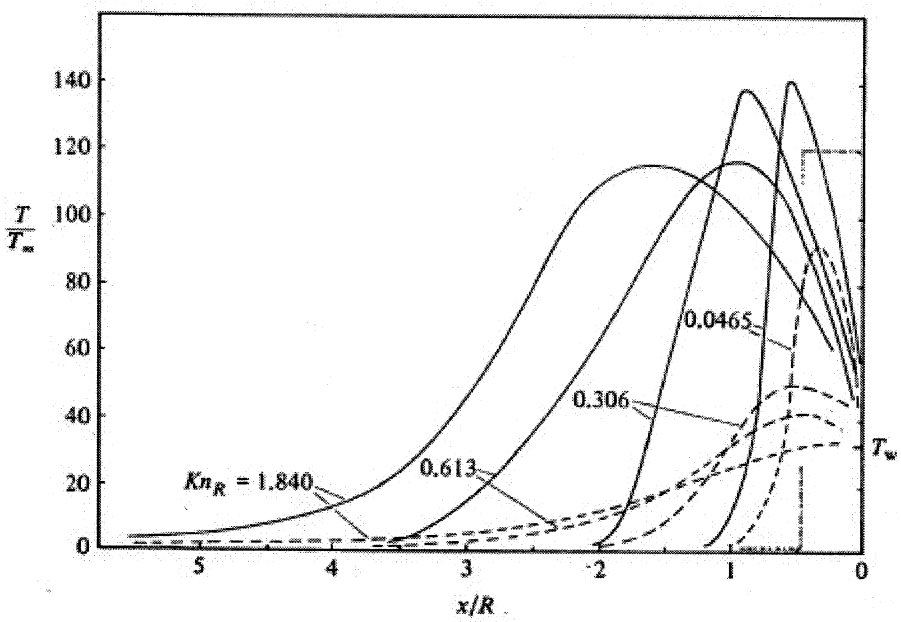

FIGURE 7. Computed near-axis temperature profiles for a blunt-ended cylinder, corresponding to figure 6: ——, translational temperature; – – –, rotational temperature; —·—·—, continuum inviscid result, $\gamma = 1.4$.

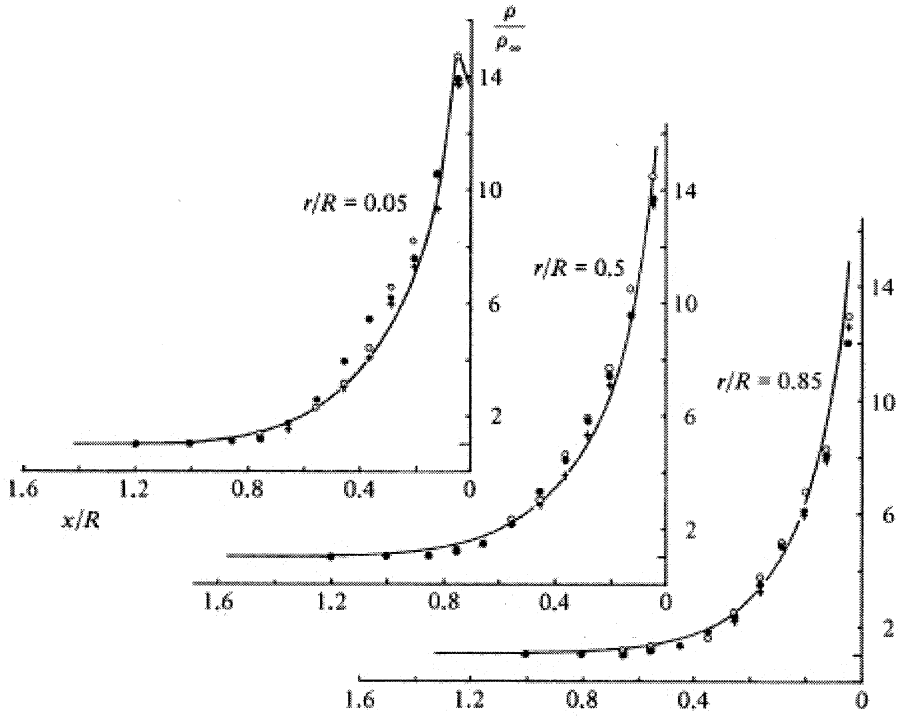

FIGURE 8. Streamwise density profiles for a blunt cylinder. $M_\infty = 25.4$, $Kn_R = 0.0648$, $T_w/T_0 = 0.26$, $T_0 = 1383$ K. Experimental data; ——. Computed data: ○, hybrid Morse potential; ●, variable-ϕ Morse potential; +, variable-ϕ inverse-power potential.

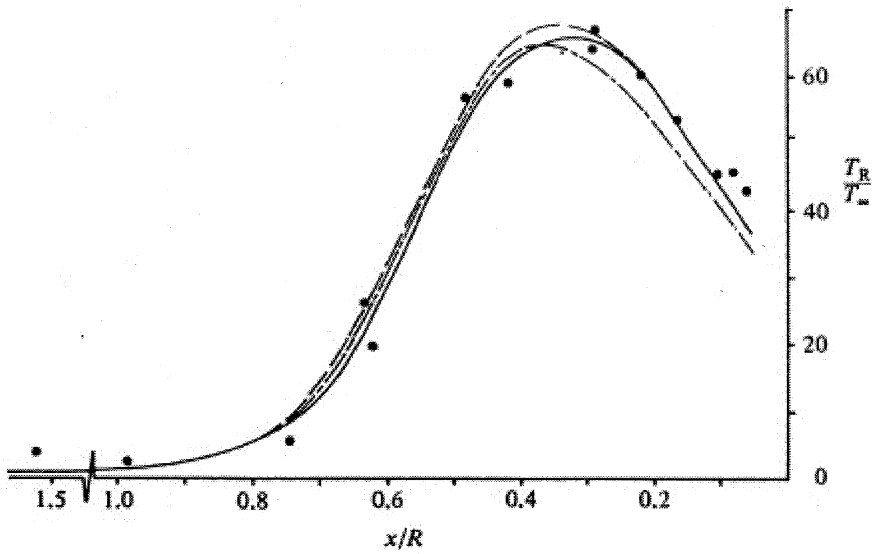

FIGURE 9. Streamwise rotational temperature profiles near stagnation line for a blunt-ended cylinder. $M_\infty = 20.6$, $Kn_R = 0.0282$, $T_w/T_0 = 0.26$, $T_0 = 1405$ K. Experimental data, $r/R = 0$: ●. Computed data, $r/R = 0.1$: – – –, hybrid Morse potential; ——, variable-ϕ Morse potential; – – –, variable-ϕ inverse-power potential.

inelastic cutoff to both the Morse and inverse-power potentials. This will make the inelastic-collision rate for the two models similar. This modified model was used and compared with a new experiment to measure the rotational temperatures. For unavoidable reasons, this was not conducted at the same free-stream conditions as the density survey. The Mach number was 20.6 and the Knudsen number was 0.0282.

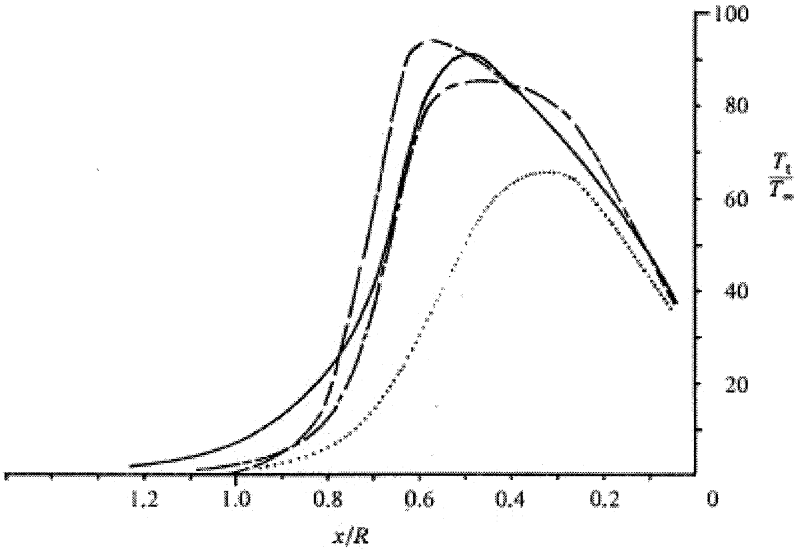

FIGURE 10. Streamwise translational temperature profiles near stagnation line for blunt-ended cylinder. Key to collision models and flow conditions as figure 9. ..., T_R for variable-ϕ Morse potential.

The flow field was therefore recalculated for the three collision models. The density profiles were similar to those in figure 8, but the differences between the Morse and inverse-power potentials were reduced, presumably as a consequence of adjusting the cross-section for inelastic collisions.

The rotational temperature results from the calculations and the experiment (which were performed quite independently) are shown in figure 9, and agree very well. Figure 10 shows the corresponding translational temperature profiles and it can be seen that each scattering model gives a different standoff distance for the temperature 'shock'. The translational temperatures were not measured, so we cannot judge the relative merits of the scattering potentials from this. The difference between the translational temperature and the rotational temperature is a measure of the amount of energy that is available to be transferred from translational to rotational modes by collisions. If Z_R was constant, that is if the average amount of energy transferred was independent of the energy of collision, we would expect the rotational modes by collisions. If Z_R were constant, that is if the average amount of energy transferred were independent of the energy of collision, we would expect the the T_R profiles are not markedly different before they peak. Thus the variations in Z_R in some way compensated for the variation in position of the thermal shock. It would be expected from this that a constant-ϕ scheme would not have worked as well here.

After the peak of rotational temperature, the hybrid exchange gives results clearly different from those for the variable-ϕ and not quite so good. It is known that the hybrid model does not achieve equipartition at equilibrium and this can be seen as the two temperatures approach the wall temperature. The rotational temperature profiles indicate that the Morse-potential variable-ϕ combination is marginally the best. Clearly these conclusions are based on sparse experimental evidence, all of which is subject to error, and some caution should be exercised.

7. Conclusions

The Monte Carlo direct simulation method has been used to calculate contrasting rarefied hypersonic flows produced by two body shapes for a range of Knudsen numbers. Different intermolecular collision models, which are computationally viable for complex flows, have been tested and the results compared with wind-tunnel measurements for the equivalent flows. Good agreement between measured and calculated density and temperature profiles has been achieved.

For the flow ahead of a blunt cylinder, successful predictions of the measured flow density and rotational temperature have been obtained. The most accurate agreement with density profiles ahead of the front face, where rapid compression occurs, is obtained using the simplest model, a phenomenological variable-ϕ energy transfer and inverse-power scattering. The other models showed some discrepancies where the rotational temperature was climbing rapidly towards equilibrium with the translational mode. However, for the Morse-potential/variable-ϕ combination, it appears that the choice of inelastic cutoff was responsible for some of this discrepancy. The rotational temperature profile close to the stagnation streamline showed that the hybrid scheme, in which high-relative-energy encounters are modelled classically and which displays a variation of Z_R with temperature, gave reasonable results where the flow was far from equilibrium. The results were poorer as the flow approached equilibrium since this model is unable to satisfy equipartition. The variable-ϕ model, which effectively achieves equipartition, gave an accurate representation of the internal energy transfer in the rapidly compressing flow. It appears likely that if ϕ were constant the results would not have been so good.

For the hollow-cylinder flow, which is the axisymmetric equivalent of a flat plate, a trade-off between speed and accuracy of the collision algorithm has been seen. The simplest and quickest, the inverse-power variable-ϕ routine, gave tolerable results. By adjusting the disposable constants α and β in the inverse-power potential we could have obtained better results. The constants can be chosen to give a good fit with viscosity for the range of temperature which is thought in advance to be appropriate. However, since the viscosity is a near-equilibrium property it is possible that the model will give unquantifiable discrepancies far from equilibrium. There is also the slight disadvantage that, since the inelastic collision rate is altered each time new constants α and β are chosen, the variable-ϕ equation has to be rederived. This task can be reduced by relating ϕ to Z_R through Pullin's (1978) theory. Although this is based on a statistical model slightly different from the restricted exchange scheme used here, he has obtained reasonable agreement for $\alpha = \infty$ (hard spheres) as have we for $\alpha = 13.5$.

The Morse potential offers better hope of being a general-purpose model. This, with about a 15 % cost in computing time (due to the larger collision cross-section), includes both repulsive and attractive forces and the latter are important in relatively low-energy encounters. Since it gives a better representation of the actual forces between molecules it should be able to give accurate results over a wider range of conditions than the inverse-power potential. When this model is applied to the hollow-cylinder flow, the structure of the non-Rankine shock and the viscous layer beneath it are predicted accurately. Further slight improvements are obtained, at some computing cost, when the variable-ϕ model is replaced by Pullin's hybrid model to give an appropriate correlation between pre- and post-collision properties. This suggests that a more rigorous statistical model might be sought which also retains this sort of correlation. The statistical exchange schemes can be criticized for reasons similar to

those mentioned for the inverse-power potential. It is only by matching near-equilibrium measurements of Z_R that we can establish the appropriate value of ϕ. The variable-ϕ equation with inelastic cutoff for 'weak' collisions goes a little way towards a 'realistic' exchange model that would work well far from equilibrium. It would probably be desirable to make the exchange restriction factor a more sophisticated function of $b(mg^2/2\alpha\beta)^{1/\alpha}$ than the simple cutoff now used. The relation between ϕ and Z_R for any functional dependence can be established from Pullin's theory.

Because of its versatility the Morse potential combined with the variable-ϕ energy exchange is recommended as a general-purpose collision model.

REFERENCES

Bird, G. A. 1970*a* Breakdown of translational and rotational equilibrium in gaseous expansions. *AIAA J.* **8**, 1998.

Bird, G. A. 1970*b* Numerical simulation and the Boltzmann equation. In *Rarefied Gas Dynamics, 7th Symp.*, vol. II (ed. Dini), p. 693.

Bird, G. A. 1976 *Molecular Gas Dynamics*, Clarendon.

Borgnakke, C. & Larsen, P. S. 1973 Statistical collision model for Monte-Carlo simulation of polyatomic gas. *Dept Fluid Mech., Tech. Univ. Denmark, Lyngby*, Rep. AFM 73–08.

Carnevale, E. H., Cary, C. & Larsen, G. 1967 Ultrasonic determination of rotational collision numbers and vibrational relaxation times of polyatomic gases at high temperatures. *J. Chem. Phys.* **47**, 2829.

Davis, J. 1978 An experimental study to evaluate and develop the direct simulation method as applied to rarefied hypersonic flow fields. Ph.D. thesis, Aero. Dept, Imp. Coll., London.

Davis, J. & Harvey, J. K. 1979 A digital technique for conditioning spectrometer data. *J. Phys.* E: *Sci. Instrum.* **12**, 25.

Deiwert, G. S. & Yoshikawa, K. K. 1975 Analysis of a semi-classical model for rotational transition probabilities. *Phys. Fluids* **18**, 1085.

Harvey, J. K., Jeffery, R. W. & Uffington, D. C. 1971 The Imperial College Graphite Heated Hypersonic Wind Tunnel. *British ARC R&M* 3701.

Hirschfelder, J. O., Curtiss, C. F. & Bird, R. B. 1965 *Molecular Theory of Gases and Liquids*, 2nd edn. Wiley.

Itikawa, Y. & Yoshikawa, K. K. 1975 Monte-Carlo calculations of diatomic molecule gas flows. *NASA Ames Research Centre* TND 8100.

Larsen, P. S. & Borgnakke, C. 1974 Statistical collision model for simulating polyatomic gas with restricted energy exchange. In *Rarefied Gas Dynamics, 9th Symp.*, vol. I (ed. Becker & Fiebig), Paper A7, DFVLR Press, Porz-Wahn, Germany.

Lordi, J. A. & Mates, R. E. 1970 Rotational relaxation in nonpolar diatomic gases. *Phys. Fluids* **13**, 291.

Macpherson, A. K. 1971 Rotational temperature profiles of shock waves in diatomic gases. *J. Fluid Mech.* **49**, 337.

Melville, W. K. 1972 The use of the loaded sphere molecular model for computer simulation of diatomic gases. *J. Fluid Mech.* **51**, 571.

Morse, P. M. 1929 Diatomic molecules according to the wave mechanics. II. Vibration levels. *Phys. Rev.* **34**, 57.

Muntz, E. P. 1961 Measurement of rotational temperature, vibrational temperature and molecular concentration, in non-radiating flows of low density nitrogen. *Inst. Aerophys., Univ. Toronto, UTIA Rep.* 71.

Parker, J. G. 1959 Rotational and vibrational relaxation in diatomic gases. *Phys. Fluids* **2**, 449.

Pearson, W. E. & Hansen, C. F. 1972 Collision induced rotational transition probabilities in diatomic molecules. In *Rarefield Gas Dynamics, 8th Symp.* (ed. K. Karamcheti), p. 167. Academic.

PULLIN, D. I. 1974 Rarefied leading edge flow of a diatomic gas. Ph.D. thesis, Aero. Dept, Imp. Coll., London.

PULLIN, D. I. 1975 Model kinetic equations for structureless polyatomic molecules with phenomenological energy exchange. *Aero. Dept, Imp. Coll., London Rep.* 75–10.

PULLIN, D. I. 1978 Kinetic models for polyatomic molecules with phenomenological energy exchange. *Phys. Fluids* **21**, 209.

PULLIN, D. I. & HARVEY, J. K. 1976 A numerical simulation of the rarefied hypersonic flat plate problem. *J. Fluid Mech.* **78**, 689.

VINKOUR, M. 1959 Hypersonic flow around bodies of revolution which are generated by conic sections. in *Proc. 6th Midwestern Conf. on Fluid Mech.*, p. 232. University of Texas Press.

WOOLLEY, H. W. 1956 Thermodynamic properties of gaseous nitrogen. *NACA* TN 3271.